In situ immunomodulation of tumors with biosynthetic bacteria promote anti-tumor immunity

Zhongda Lin [a,1], Fanqiang Meng [a,1], Yumeng Ma [a,1], Chi Zhang [a], Zhirang Zhang [a], Zhaoxin Yang [a], Yuan Li [a], Linlin Hou [a], Yuzhong Xu [c], Xin Liang [b], Xudong Zhang [a,*]

[a] *Shenzhen Key Laboratory for Systems Medicine in Inflammatory Diseases, School of Medicine, Shenzhen Campus of Sun Yat-Sen University, Sun Yat-Sen University, Shenzhen, 518107, Guangdong, China*
[b] *Guangdong Provincial Key Laboratory of Medical Molecular Diagnostics, Key Laboratory of Stem Cell and Regenerative Tissue Engineering, School of Basic Medical Sciences, Guangdong Medical University, Dongguan, 523808, China*
[c] *Department of Clinical Laboratory, Shenzhen Baoan Hospital, The Second Affiliated Hospital of Shenzhen University, Shenzhen, 518101, China*

ARTICLE INFO

ABSTRACT

Immune checkpoint blockade (ICB) therapy potently revives T cell's response to cancer. However, patients suffered with tumors that had inadequate infiltrated immune cells only receive limited therapeutic benefits from ICB therapy. Synthetic biology promotes the alternative strategy of harnessing tumor-targeting bacteria to synthesize therapeutics to modulate immunity *in situ*. Herein, we engineered attenuated *Salmonella typhimurium* VNP20009 with gene circuits to synthesize granulocyte-macrophage colony-stimulating factor (GM-CSF) and interleukin 7 (IL-7) within tumors, which recruited dendritic cells (DCs) and enhanced T cell priming to elicit anti-tumor response. The bacteria-produced GM-CSF stimulated the maturation of bone marrow-derived dendritic cells (BMDCs), while IL-7 promoted the proliferation of spleen isolated T cells and inhibited cytotoxicity T cell apoptosis *in vitro*. Virtually, engineered VNP20009 prefer to colonize in tumors, and inhibited tumor growth by enhancing DCs and T cell infiltration. Moreover, the tumor-toxic GZMB$^+$ CD8$^+$ T cell and IFN-γ^+ CD8$^+$ T cell populations conspicuously increased with the treatment of engineered bacteria. The combination of GM–CSF–IL-7-VNP20009 with PD-1 antibody synergistically stunted the tumor progress and stasis.

1. Introduction

Immune checkpoint blockade (ICB) therapy that mainly employ the blocking antibody to disrupt the immunosuppressive checkpoint on the exhausted T cells to revive their response to cancers [1–3]. Although antibodies targeting cytotoxic T lymphocyte antigen 4 (CTLA-4) and the programmed cell death protein 1 (PD-1) have been approved for treating multiple type of cancers, the majority of the patients who suffering from 'cold' tumors achieved poor response to ICB therapy [4,5]. 'Cold' tumors always are described with few lymphocytes infiltration, low checkpoint ligands expression and lack of tumor antigen expression [6]. In addition, hypoxia of the tumor microenvironment (TME) recruits the immunosuppressive suppressor cell such as myeloid-derived suppressor cells (MDSC) and M2 macrophages infiltrating into the tumor [5,7–9]. Intriguingly, oncolytic viruses (OVs) have unique abilities to specifically lyse tumor cells and recruit DCs, and are considered function as tumor vaccines [10,11]. Currently, oncolytic virus has been devised to express immunostimulatory molecules including GM-CSF, CD40L, OX40L or PD-1 antibody which could further enhance the recruitment of DCs and priming of T cells [12,13]. More importantly, recent studies have proved that the synergistic anti-tumor effects of OVs combine with immune checkpoint antibodies could significantly promote the potency of ICB therapy [14–16]. However, the dearth of tumor-targeting ability and consequent anti-viral response are the major hurdles of the administration of OVs [17,18]. Thus, OVs are always directly injected into epidermal tumors such as melanoma currently, which seriously restrains the application of OVs in other types of cancer [19].

Recently, a variety of bacteria are isolated from multiple tumors, demonstrating that bacteria may be closely related to tumor progression [20,21]. Actually, as early as the 1800s, William B. Coley had discovered

that the injection of streptococcal organisms shrank the malignant tumor [22]. And in the 1970s, bacillus Calmette–Guérin (BCG), an attenuated *Mycobacterium bovis* strain, was approved to treat bladder cancer [23]. Hereafter, attenuated strains such as *Listeria*, *Clostridium*, *Escherichia coli* and *Salmonella* were widely developed to synthesize cytokines, toxic proteins and immune checkpoint antibodies for cancer therapy [24–29]. After intravenous injection, the bacteria target and proliferate within tumor hypoxic core, which finally induces tumor cell death and elicits host's innate and adaptive immune response [30–32]. VNP20009 is an attenuated *Salmonella typhimurium* that knocks out the *msbB* and *purI* genes, achieving remarkable tumor targeting and inhibition effects in mouse models [24,33]. Knocking out the *msbB* gene results in the loss of myristoylation of the lipid A component of *Salmonella* LPS, which dampen the LPS-induced TNF release, significantly reducing the risk of host septic shock. Further knocking out the *purI* gene leads to purine synthesis defects in VNP20009, which make the bacteria only colonizes in purine rich tumor environments but not healthy tissues [24,33]. *Salmonella* does not have strong activity to kill tumor cells directly, and its anti-tumor activity mainly because of immune activation. *Salmonella* infection causes tumor cells to up-regulate the expression of gap junction protein Cx43, enhancing the gap junction between DCs and tumor cells, and promoting DCs to phagocytose tumor cells. Meanwhile, tumor cells down-regulate the expression of indoleamine 2,

3-dioxygenase (IDO), which is beneficial for the activation of CD8+ T cells. The *Salmonella* LPS can activate the LPS receptor (CD14) and Toll like receptor 4 (TLR4) on macrophages, which induces TNF secretion, and subsequently damages tumor blood vessels. In addition, the flagella protein (Flagellin) of *Salmonella* also has multiple immune activation effects: stimulating natural killer (NK) cells to produce IFN-γ, perforin and granzyme, reducing the frequency of CD4+ CD25+ Treg cells in tumors, enhancing activity of CD8+ T cells through Toll like receptor 5 (TLR5) signaling [33,34]. More importantly, the rapid progression of synthetic biology endows the harness of bacteria as bioreactors to synthesize the therapeutics to eradicate tumor cells *in situ* [35,36]. Engineered bacteria with gene circuits containing sensor elements can respond to the biomarkers in TME like hypoxia, low pH, or external ultrasonic, optothermal and chemical inducers, then output the therapeutics such as immune checkpoint antibodies, immune cytokines, and L-Asparaginase [31,37–43].

Anaerobic bacteria has offered a new approach to tumor therapy, due to its tumor targeting, replication and genetic stability in tumor tissues and anti-tumor effects *in vivo*. Meanwhile, the development of synthetic biology provides powerful tools for designing, modifying and controlling the biological activities of bacteria. Herein, we engineered an attenuated *Salmonella typhimurium* VNP20009, a *purI* and *msbB* gene excision strain, to synthesize and secrete GM-CSF and IL-7 in orthotopic
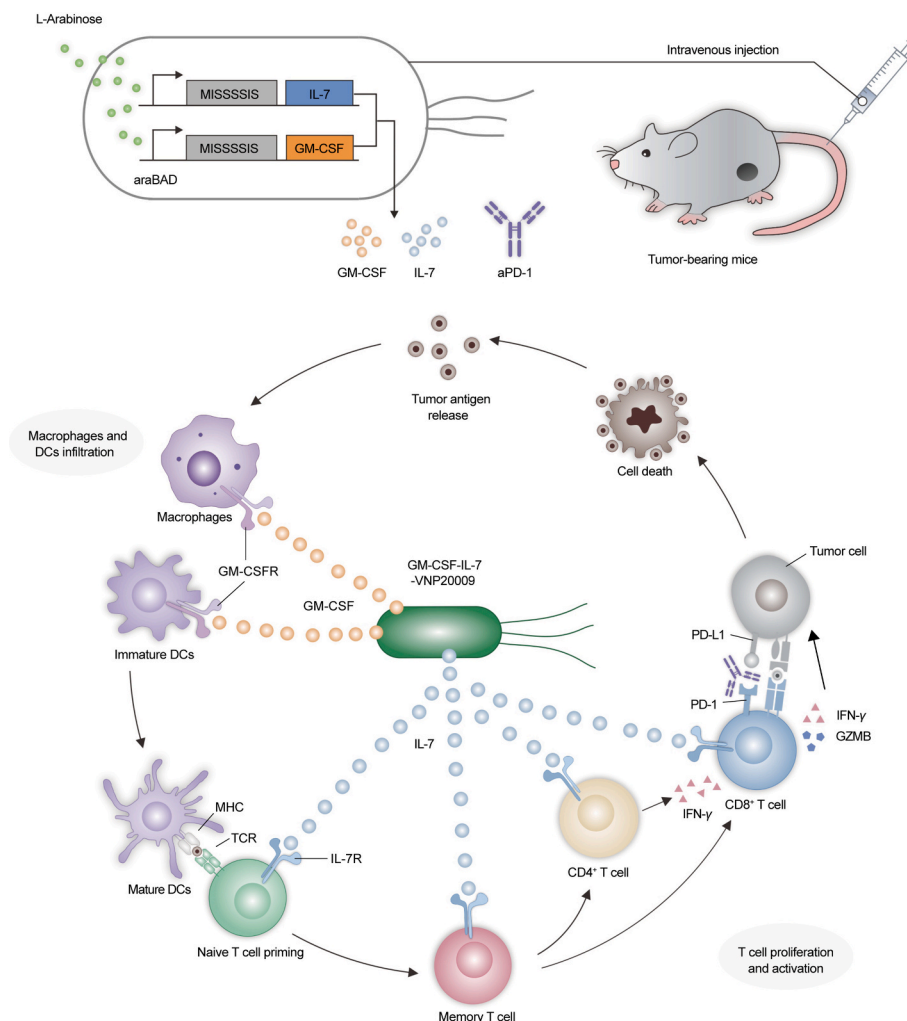
Schematic. The schematic presents the construction of GM–CSF–IL-7-VNP20009 strain and the mechanism of GM–CSF–IL-7-VNP20009 in stimulating systematic anti-tumor immunity. After intravenous injection, GM–CSF–IL-7-VNP20009 targets and colonizes within tumor hypoxic core. When is given L-Arabinose, GM–CSF–IL-7-VNP20009 secretes the GM-CSF and IL-7 fusion proteins *in situ*. GM-CSF promotes the recruitment and maturation of macrophages and DCs, while IL-7 enhances the proliferation and activation of naive T cells, memory T cells and effector T cells. Additional PD-1 antibody (aPD-1) disrupts the PD-1/PD-L1 axis and protects T cells from exhaustion.

tumor [44]. GM-CSF is certified to recruit monocytes, macrophages and DCs in TME [45–47] and approved to assist tumor elimination by the FDA [48]. Moreover, IL-7 is crucial for the survival of resting T cells including naïve T cells and memory T cells [49,50] and is widely used as an adjuvant of cancer vaccines [51]. Tumor colonized bacteria secreted GM-CSF *in situ*, that recruited macrophages, DCs and promoted T cell priming. Subsequently, the bacteria-secreted IL-7 stimulated tumor-specific effector T cell and memory T cell expansion. Moreover, co-administration of PD-1 antibody (aPD-1) disrupted PD-1/PD-L1 axis protecting T cells from exhaustion, intensively potentiated systematic anti-tumor immunity. Collectively, GM-CSF, IL-7 and aPD-1 worked together to activate the anti-tumor immune circuits (Schematic).

2. Materials and methods

2.1. Preparation of GM–CSF–IL-7-VNP20009

First, we prepared the VNP20009 competent bacteria. The monoclonal VNP20009 was cultured in 50 mL LB medium. When OD_{600} of the broth reach 0.4–0.6, the broth was placed on ice for 30 min. After the ice bath, the bacteria were collected by 4000 rpm centrifugation for 10 min at 4 °C. Discarded the supernatant, and resuspended the bacteria with 10 mL ice cold sterilized ddH_2O. Collected the bacteria by 4000 rpm centrifugation for 10 min at 4 °C, then gently resuspend the bacteria with 10 mL 10% ice cold sterilized glycerol and stand on ice for 10 min. Repeated the previous step and then gently resuspend the bacteria with 1 mL 10% ice cold sterilized glycerol. Precooled 10 1.5 mL centrifuge tubes on ice and added 100 μL competent bacteria into each centrifuge tube. Quickly plunged the centrifuge tubes into liquid nitrogen for snap freezing. The competent bacteria were preserved at −80 °C.

Secondly, we inserted the mouse GM-CSF and IL-7 gene sequences into the MCS region of pBAD-HA and pBAD-Flag plasmids respectively. In addition, we inserted the nucleotide sequence of the *Salmonella* secretion system signal peptide at the N-terminal of GM-CSF and IL-7 to control their secretion. The nucleotide sequences for inserting the plasmids were provided in supplementary file (Table 1).

Thirdly, the pBAD-GM–CSF–HA and pBAD-IL-7-Flag plasmids were electroporated into VNP20009 competent bacteria. Unfroze VNP20009 competent bacteria on ice, added 1 μg plasmid, gently mix well and stand on ice for 20 min. Quickly transferred the competent bacteria mixture to the frozen electric shock cup and electroporated at Ec1 for two times. Added 800 μL SOC medium to wash out the bacteria from electric shock cup, cultured in 37 °C for 1 h. Finally, performed resistance screening and gene sequencing on the transformed bacteria. The stable strains were maintained in LB medium containing 100 μg/mL ampicillin and 50 μg/mL kanamycin at 37 °C. 2% L-arabinose was used to induce the secretion of GM-CSF and IL-7.

2.2. SDS-PAGE assay

Bacterial pellets and culture supernatants were collected by centrifuge at 4 °C, 4500 r.p.m. The bacterial pellets were lysed with 20 mg/mL lysozyme at room temperature for 20 min. Both the bacterial lysate and culture supernatant was sonicated on ice for 2 min. Additionally, the culture supernatant was concentrated with ultrafiltration (Millipore, 10K NMWL) tubes. The tumor tissues were homogenized and lysed with RIPA buffer. 10% polyacrylamide gels were used for electrophoresis and then we transformed the proteins to PVDF membranes. After 60 min of blocking in 5% non-fat dry milk, the PVDF membranes were incubated with the first antibodies against HA-Tag (Abmart, M20003), Flag-Tag (Cell Signaling Technology, 14793), GM-CSF (Abmart, PA2949), IL-7 (Abmart, TD6530) and *β*-Tubulin (Abmart, M20005) at 4 °C overnight. The PVDF membranes were washed three times with TBST buffer for 5 min and then incubated with secondary antibodies for 1 h at room temperature. Before analyzing with enhanced chemiluminescence detection (ECL), the PVDF membranes were finally washed three times

with TBST buffer for 5 min.

2.3. Immunofluorescence assay

The bacteria were collected, washed with PBS, and then fixed in 4% paraformaldehyde for 15 min at room temperature. Next, the bacteria were resuspended in 3% bovine serum albumin (BSA) containing 4% Triton X-100 and incubated for 10 min on ice. The bacteria were incubated with 1:100 diluted primary antibodies against HA-Tag (Abmart, M20003), Flag-Tag (Cell Signaling Technology, 14793), GM-CSF (Abmart, PA2949) and IL-7 (Abmart, TD6530) at 37 °C for 2 h. After washing bacteria with PBS, the bacteria were incubated with 1:200 diluted Alexa Fluor® 594-conjugated Goat Anti-Mouse IgG (abcam, ab150116) and Alexa Fluor® 488-conjugated Goat Anti-Rabbit IgG (abcam, ab150077) for 1h at 37 °C. Finally, the bacteria were stained with DAPI for 10 min at room temperature and prepared for analysis. The tumor samples were firstly fixed in 4% paraformaldehyde overnight and frozen in optimal cutting temperature (OCT) compound. The frozen tissues were cut into 6 μm thick slices and adhered to glass slides. The tumor slices were washed in PBS for 15 min to remove the OCT compound and boiled in antigen retrieval solution for 20 min. After natural cooling-off, the slides were incubated with 3% BSA for 1h then incubated with CD4 antibody (1:100 dilution, abcam, ab183685), CD8 antibody (1:100 dilution, abcam, ab22378) or CD11c antibody (1:100 dilution, abcam, ab33483) at 4 °C overnight. The slices were washed in PBS for three times and incubated with Alexa Fluor® 488-conjugated Goat Anti-Rabbit IgG (1:200 dilution, abcam, ab150077), Alexa Fluor® 594-conjugated Goat Anti-Rat IgG (1:200 dilution, abcam, ab150160) or Alexa Fluor® 488-conjugated Goat Anti-Armenian Hamster IgG (1:200 dilution, abcam, ab173003) for 1 h at room temperature. Finally, we washed the slices in PBS three times and stained the nucleus with DAPI for 10 min. All the samples were analyzed through confocal microscopy (Zeiss).

2.4. ELISA assay

The secretion efficiency of GM-CSF and IL-7 was detected by ELISA assay. The resistant LB medium was inoculated with 500 μL GM–CSF–IL-7-VNP20009 to 50 mL, and continued to be cultured until OD600 reached 0.4 to 0.6.2% L-arabinose was added to induced protein expression at 24 °C. 50 mL bacteria solution was collected at 4 h, 8 h, 12 h, 16 h, 24 h, 48 h and removed the bacteria with 0.22 μm filters. The induced supernatant was stored at −80 °C. After all supernatant samples were collected, detected with GM-CSF ELISA kit (70-EK263/2–96) and IL-7 ELISA kit (70-EK207/2–96).

After intravenous administration of 10^5 CFU GM–CSF–IL-7-VNP20009 per mouse, the concentration of pro-inflammatory cytokines in major organs and serum were detected by ELISA assay to evaluate the early systemic inflammation risk. The heart, liver, spleen, lung, kidney and brain tissue were harvested at 6 h, 12 h, 18 h, 24 h after bacteria administration. The tissue samples were first homogenized, and centrifuged at 14000 rpm to acquire the supernatant. All the supernatant was stored at −80 °C and finally detected with GM-CSF ELISA kit (70-EK263/2–96), IL-7 ELISA kit (70-EK207/2–96), IL-6 ELISA Kit (70-EK206/3–96) and TNF-*α* ELISA Kit (70-EK282/3–96). What's more, the serum was harvested at 0 d, 1 d, 7 d, 14 d and stored at −80 °C, finally detected with IL-6 ELISA Kit (70-EK206/3–96) and TNF-*α* ELISA Kit (70-EK282/3–96).

2.5. In vitro activity studies

Firstly, we isolated the primary cells from mice. The bone marrow cells were cultured in RPMI 1640 containing 10 ng/mL IL-4 while the spleen cells were cultured in RPMI 1640 containing 100 U/mL IL-2. The GM–CSF–IL-7-VNP20009 was induced by 2% L-Arabinose at 24 °C for 8 h, and then the induced bacterial supernatant was harvested. We used

ultrafiltration tubes (Millipore, 10K NMWL) to concentrate GM-CSF and IL-7 in the bacterial supernatant to 2 mg/mL and 1 mg/mL. Next, the bone marrow cells were co-cultured with 20 ng/mL bacteria-produced GM-CSF for 7 days while the spleen cells were co-cultured with 10 ng/mL bacteria-produced IL-7 for 48 h. Finally, the bone marrow cells were stained with APC anti-CD11c antibody (BioLegend, 117310), FITC anti-CD80 antibody (BioLegend, 104705) and PE anti-CD86 antibody (Bio-Legend, 159204) while the spleen cells were stained with FITC anti-CD3ε antibody (BioLegend, 100306) and PE anti-Ki67 antibody (Bio-Legend, 652403). All the samples were analyzed with flow cytometry.

CTLL-2 cell was a cytotoxic T lymphocyte that derived from C57BL/6 mice. We co-cultured CTLL-2 cells with 50 μM LY294002 and 10 ng/mL bacteria-produced IL-7 for 48 h. A part of the CTLL-2 cells was stained with APC anti-Annexin V antibody (BioLegend, 640920) and 7-AAD for flow cytometry analysis. And the rest of the CTLL-2 cells were lysed for western blot analysis to detect by cleaved caspase-3 antibody (abcam, ab214430) and Bcl-2 antibody (abcam, ab182858).

To ensure that the cell viability did not change significantly after co-incubation with non-GM-CSF or IL-7 components of the engineered VNP20009 culture supernatant, we detected the cell viability through CCK-8 assay after 48 h co-incubation.

2.6. In vivo biological distribution studies and blood routine examination

Firstly, 5×10^5 B16–F10 cells were inoculated in the abdomen of mice to obtain the tumor-bearing mice. And then, we injected 1×10^5 GM–CSF–IL-7-VNP20009 into C57BL/6 mice via tail vein injection. The heart, liver, spleen, lung, kidney and brain tissues of mice were collected at 6 h, 12 h, 1 d, 3 d, 5 d, 7 d,14 d and homogenized in 2 mL PBS. The supernatants were harvested through 500g centrifugation and 200 μL of the supernatants were spread to LB plates containing 100 μg/mL ampicillin and 50 μg/mL kanamycin. After incubating at 37 °C for 14 h, we counted the number of bacterial colonies on the LB plates.

In addition, we also used qPCR assay to detect the relative expression of VNP20009 16s rRNA in tissues at 12 h, 1 d, 3 d, 7 d and 14 d, which could reflect the number of VNP20009 that remain in the tissues. VNP20009 16s rRNA mRNA sequence was download form Genbank (NCBI Reference Sequence: NZ_CP007804.1). 16s rRNA-Forward (CAGATAGTTGGCCATCTGGC) and 16s rRNA-Reverse (ATCCGTAA-CAGTCTCGGC) were the two primers that used for qPCR detection. The expression of GAPDH was used as the internal reference.

After 10^5 GM–CSF–IL-7-VNP20009 were administered intravenously per mouse, we harvested the whole blood samples in sodium citrate anti-coagulant tubes at 0 d, 1 d, 3 d, 7 d, 14 d and detected the blood samples with automatic blood cell analyzer (BC-2800vet) to analyze inflammatory cell concentration.

2.7. In vivo anti-tumor studies of engineered VNP20009

The female C57BL/6 mice were purchased from the Guangdong Medical Laboratory Animal Center (Guangdong, China). All the mice were cared and performed according to the instructions and approval of the Institutional Animal Care and Use Committee of Sun Yat-sen University. 5×10^5 B16F10-luc cells were inoculated to the abdomens of female C57BL/6 mice to construct subcutaneous melanoma model. Once the tumor volumes of mice mostly reached 50–80 mm^3, the mice were randomly divided into 7 groups and received different treatments including [1] PBS [2], VNP200009 (1×10^5 CFU) [3], GM–CSF–VNP20009 (1×10^5 CFU) [4], IL-7-VNP20009 (1×10^5 CFU) [5], GM–CSF–IL-7-VNP20009 (1×10^5 CFU) [6], aPD-1 (BioLegend, 2.5 mg/kg body weight) [7], GM–CSF–IL-7-VNP20009 (1×10^5 CFU) plus aPD-1. To monitor the tumor growth, 3 mg per mouse of D-Luciferin potassium salt was injected intraperitoneally to capture the bioluminescence images every 3 days. And the tumor volumes and body weights of mice were measured every 2 days. Once the tumor volume of a mouse reached 1500 mm^3, part of the mice was sacrificed. The tumor tissues

were collected for tumor weight measured and flow cytometry analysis. The single cell suspensions of tumor tissues were stained with the following three antibodies protocols [1]: APC/Fire750 anti-CD11b antibody (BioLegend, 101262), APC anti-F4/80 antibody (BioLegend, 123116), PE/Cy7 anti-CD206 antibody (BioLegend, 141720), FITC anti-CD80 antibody (BioLegend, 104705), BV421 anti-CD86 antibody (BioLegend, 105032) [2], BV605 anti-CD11c antibody (BioLegend, 117334), APC/Fire750 anti-CD80 antibody (BioLegend, 104740), BV421 anti-CD86 antibody (BioLegend, 105032) [3], FITC anti-CD3ε antibody (BioLegend, 100306), PE anti-CD4 antibody (BioLegend, 100408), APC/Fire750 anti-CD8α antibody (BioLegend, 100766) [4], FITC anti-CD3ε antibody (BioLegend, 100306), PE anti-CD4 antibody (BioLegend, 100408), APC/Fire750 anti-CD8α antibody (BioLegend, 100766), BV421 anti-Ki67 antibody (BioLegend, 652411) [5], FITC anti-CD3ε antibody (BioLegend, 100306), APC/Fire750 anti-CD8α antibody (BioLegend, 100766), PE anti-Granzyme B antibody (Bio-Legend, 372208), PE/Cy7 anti-TNF-α antibody (BioLegend, 506324), BV421 anti–IFN–γ antibody (BioLegend, 505829), APC anti-Perforin antibody (BioLegend, 154304). We sacrificed some mice on day 20 and harvested their tumor tissues and major organs for immunofluorescence staining and H&E staining analysis, respectively.

In addition, 1×10^5 B16F10-luc cells were injected intravenously to the female C57BL/6 mice to construct lung metastatic melanoma model. The mice were randomly divided into 7 groups as same as those in subcutaneous melanoma model study. The tumor progression was evaluated by *in vivo* imaging. The body weight and survival of mice were recorded during treatment. The lungs of each group were dissected at 15 days after administration, and the number of lung metastasis was counted. Lung tissue H&E staining was performed to evaluate the severity of melanoma cell invasion. At the same time, we also harvested the whole blood of mice, detected the number of circulating Trp-2 specific CD8$^+$ T cells through Trp-2 specific MHC tetramer (Biolegend, 280061).

2.8. Data analysis

All data results are based on the mean ± standard deviation (mean ± SD). The statistical software SPSS 16.0 was used to compare the differences in each group. Student's *t*-test was used for analyzing the differences between two groups. One-way analysis of variance (ANOVA) was used for analyzing the differences between three or more groups, and Tukey was used for test correction. The survival curves were compared with Log-Rank (Mantel-Cox) analysis. *$P < 0.05$, **$P < 0.01$, ***$P < 0.001$, ****$P < 0.0001$. The used statistical method was indicated in the figure legend. The all n in the figure legends represented the number of biological replicates.

3. Results

3.1. GM–CSF–IL-7-VNP20009 was capable of secreting target proteins

In order to engineer VNP20009 to express GM-CSF and IL-7 proteins, we inserted the gene sequences of mouse GM-CSF and IL-7 into pBAD vector. The expression of GM-CSF and IL-7 was responded to the L-arabinose induction. Additionally, we also inserted a *Salmonella* secretory signal sequence at the N-terminus to mediate extracellular secretion of the target protein [52]. What's more, HA and Flag tags were added at the C-terminus of GM-CSF and IL-7 to facilitate bacteria-produced fusion protein detection, respectively. Afterward, we transformed the constructed plasmids into VNP20009 through electroporation and the transformed bacteria were screened by kanamycin or ampicillin, respectively. After being induced with 2% L-arabinose for 4 h at 25 °C, we harvested the bacterial pellets and culture supernatants. Next, the expression of GM-CSF and IL-7 proteins in engineered bacteria were detected by western blot and immunofluorescence staining assay. Of note, the GM-CSF and IL-7 were expressed in the engineered VNP20009

as indicated (Fig. 1A, Figs. S1A and B, Fig. S2). The western blot analysis also confirmed that the GM-CSF and IL-7 fusion proteins were successfully expressed and secreted into the culture supernatants of the engineered VNP20009 (Fig. 1B and C).

Moreover, we also explored the protein-secreting efficiency of GM–CSF–IL-7-VNP20009. As shown in Fig. 1C, the concentrations of GM-CSF and IL-7 in the culture supernatant gradually increased within 8 h, decreased from 8 h to 24 h, and stabilized from 24 h to 48 h *in vitro*. This might be due to the rapid growth of bacteria in the early stage of induced expression and the vigorous secretion of target proteins. But at the later stage, the secretion of the target protein was reduced maybe because of bacteria aging. The concentration of GM-CSF in the culture supernatant was 300–600 pg/mL, while the concentration of IL-7 was 1000–2000 pg/mL (Fig. 1D and E). The accumulated concentration of both proteins was sufficient to produce cellular effects.

Finally, we explored the GM-CSF and IL-7 secretion by GM–CSF–IL-7-VNP20009 within tumors. The tumor-bearing mice were intravenously injected with 10^5 GM–CSF–IL-7-VNP20009. And after 24 h, the mice were treated with 200 μL 20% L-arabinose. After 48 h, the tumors were harvested for western blot and immunofluorescence staining analysis. Notably, GM-CSF and IL-7 proteins were detected in the tumor of mice treated with GM–CSF–IL-7-VNP20009 (Fig. 1F). What's more, the immunofluorescence images of tumor tissues demonstrated the successful secretions of GM-CSF and IL-7 within tumors (Fig. S3).

3.2. GM–CSF–IL-7-VNP20009-secreted proteins had their biological activity in vitro

GM-CSF plays a pivotal role in the differentiation of bone marrow-derived dendritic cells (BMDCs) from murine hemopoietic progenitors, and these BMDCs highly express CD11c [53,54]. To explore whether the GM-CSF generated from GM–CSF–VNP20009 and
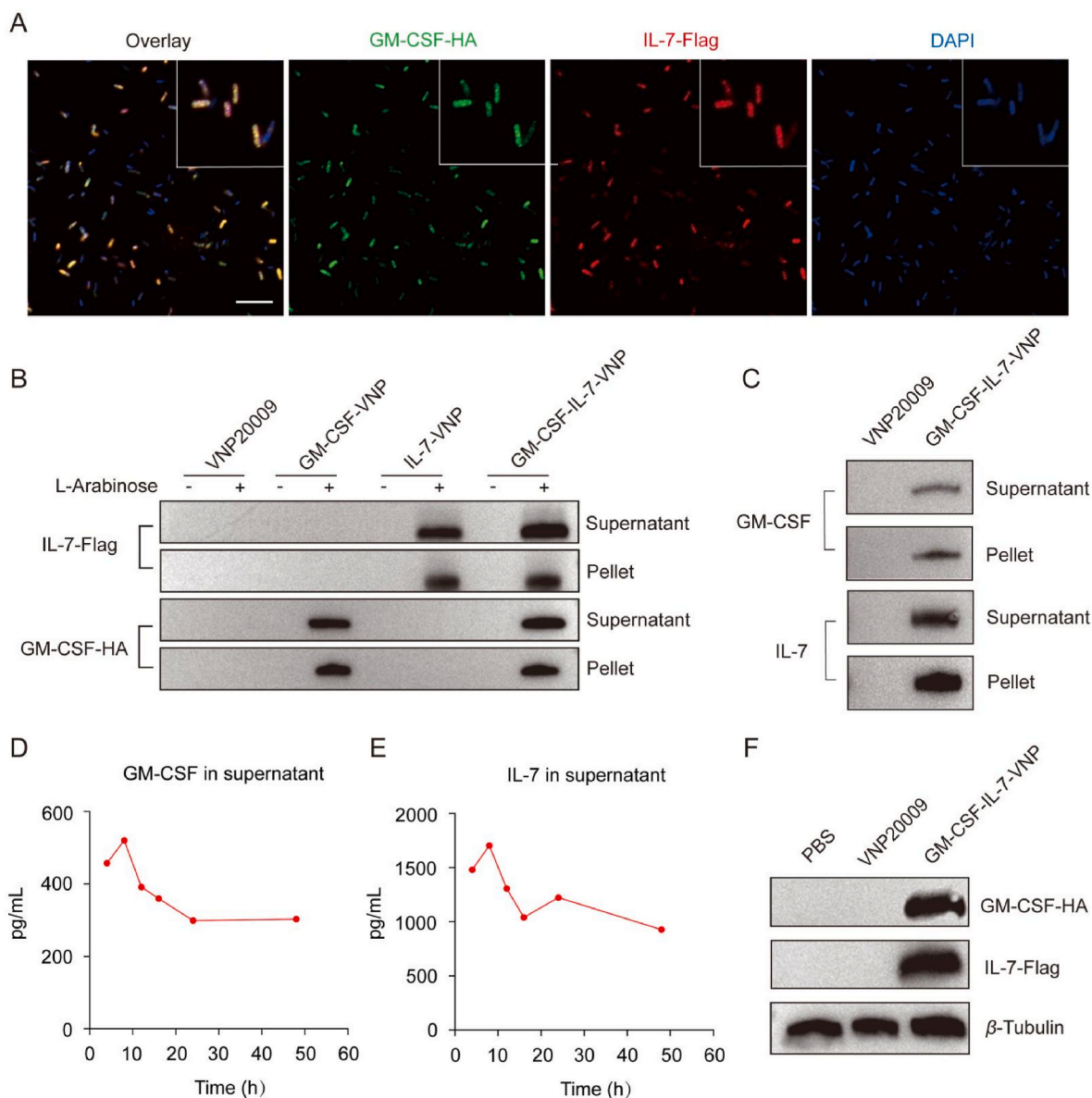
Fig. 1. GM-CSF-IL-7-VNP20009 was capable of secreting target proteins. (A) Immunofluorescence images showed the GM-CSF and IL-7 protein on GM–CSF–IL-7-VNP20009. (Scale bar: 10 μm). **(B)** Western blot analysis with HA and Flag antibodies demonstrated the successful expression and secretion of GM-CSF and IL-7 protein in engineered VNP20009. VNP is abbreviation of VNP20009 in the figures. **(C)** Western blot analysis with GM-CSF and IL-7 antibodies showed the GM-CSF and IL-7 on GM–CSF–IL-7-VNP20009. **(D) and (E)** Detection of GM-CSF and IL-7 protein that was secreted to the culture supernatants. **(F)** Western blot analysis confirmed that the intravenously administered GM–CSF–IL-7-VNP20009 could secret GM-CSF and IL-7 within tumors.

GM–CSF–IL-7-VNP20009 have the biological activity, the bacteria culture supernatant was incubated with the mouse bone marrow cells. We used CD11c, CD80, CD86 antibodies to gate the mature bone marrow-derived dendritic cells (BMDCs). Remarkably, the percentage of BMDCs significantly increased after treating with the bacteria-secreted GM-CSF *in vitro* (Fig. 2A and B). IL-7 enhances the long-time survival and proliferation of resting T cells by activating PI3K/AKT signal pathway. The consequently upregulated Bcl-2 expression exerts anti-apoptosis function in T cells [49]. We isolated primary T cells from mouse spleen and incubated the T cells with bacteria-secreted IL-7. CD3 and Ki67 antibody were used to gate proliferative spleen T cells. After being treated with the bacteria-secreted IL-7, the percentage of Ki67$^+$ cells out of CD3$^+$ cells were significant increase (Fig. 2C and D). Furthermore, to investigate whether the bacteria-secreted IL-7 could protect T cells from apoptosis, we co-incubated the mouse cytotoxic T cell line (CTLL-2) with an apoptosis-induced PI3K inhibitor LY294002. Next, we stained CTLL-2 cells with APC-Annexin V antibody and 7-AAD to distinguish the apoptotic cells. Notably, the bacteria-secreted IL-7 could protect CTLL-2 cells from LY294002-induced apoptosis (Fig. 2E and F). In addition, purified IL-7 could induce the expression of anti-apoptosis protein Bcl-2 in CTLL-2 cells and decrease the protein level of cleaved caspase-3 that executes the cell apoptosis (Fig. 2G).
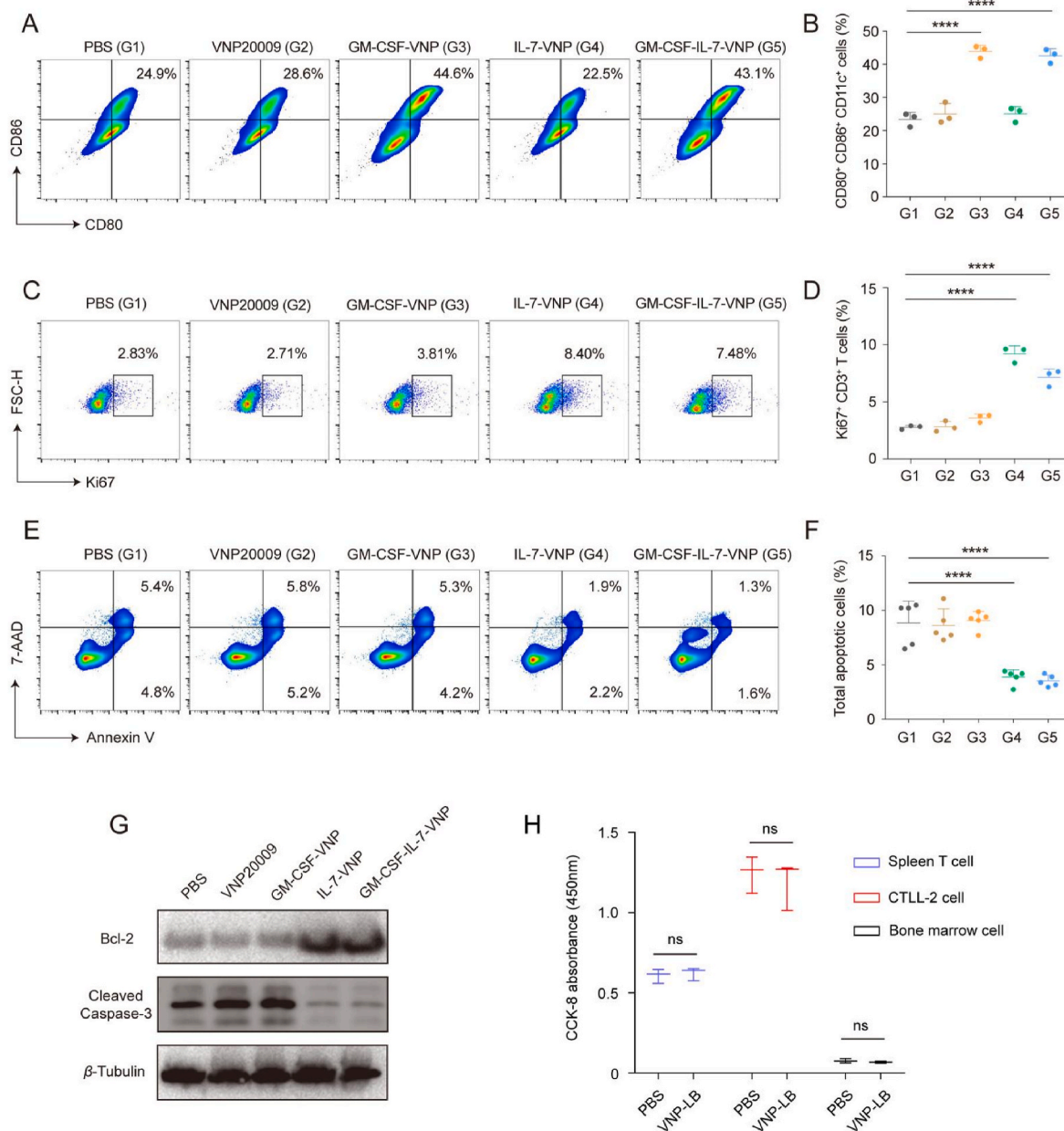
Fig. 2. GM-CSF-IL-7-VNP20009-secreted proteins had their biological activity *in vitro*. (A) and (B) Flow cytometry analysis indicated the *in vitro* activity of bacteria-secreted GM-CSF to drive mature BMDCs from mouse bone marrow cells (gated out of CD11c$^+$ cells, *n* = 3). Error bar, mean ± s.d. **(C) and (D)** Flow cytometry showed that bacteria-secreted IL-7 promoted the Ki67 expression of mouse spleen CD3$^+$ T cells (gated out of CD3$^+$ cells, *n* = 3). Error bar, mean ± s.d. **(E) and (F)** Total apoptosis rate detection by flow cytometry of CTLL-2 cells demonstrated that bacteria-secreted IL-7 protected CTLL-2 from apoptosis (gated out of total cells, *n* = 5). Error bar, mean ± s.d. **(G)** Western blot analysis explained the anti-apoptotic effect of bacteria-secreted IL-7 on CTLL-2 cells. **(H)** The cell viability of bone marrow cells, spleen cells and CTILL-2 cells was determined by CCK-8 assay after co-incubation with VNP20009 culture supernatant for 48 h (*n* = 3). Error bar, mean ± s.d. ns: no significant difference, *P < 0.05, **P < 0.01, ***P < 0.001, ****P < 0.0001. The statistics in (A) to (F) were analyzed by one-way ANOVA with Tukey test and the statistics in (H) were analyzed by Student's *t*-test.

These data suggested that the bacteria-secreted GM-CSF was able to induce mature BMDCs from mouse bone marrow cells. Meanwhile, the bacteria-secreted IL-7 could promote spleen T cell proliferation and protect T cells from apoptosis by inducing the expression of Bcl-2. CCK-8 assay showed that after 48 h co-incubation with VNP20009 culture

supernatant, there was no significant difference in cell viability of the bone marrow cells, spleen cells and CTLL-2 cells, eliminating the interference of non-GM-CSF and non-IL-7 components in the experimental results (Fig. 2H).
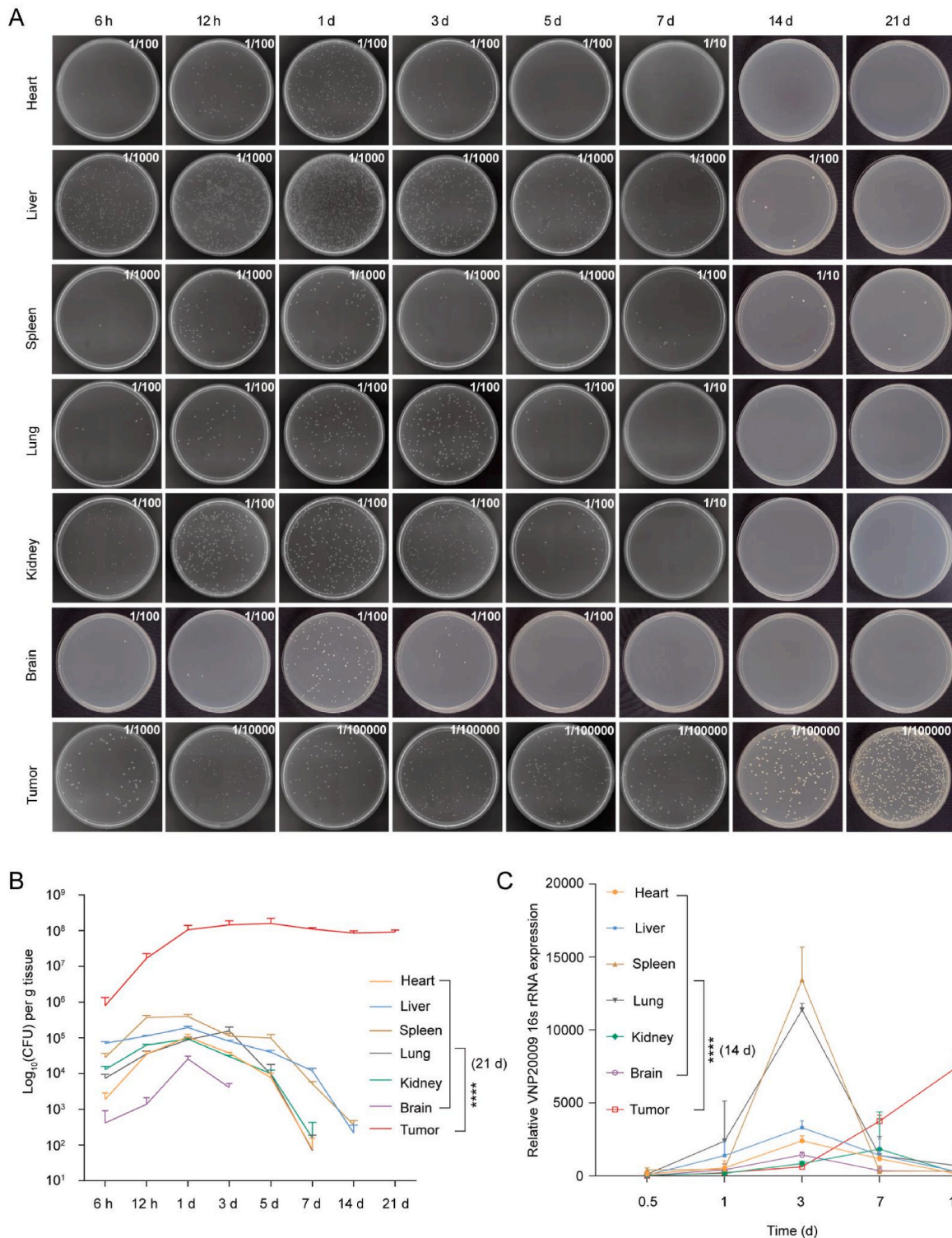
Fig. 3. **Intravenously administered GM-CSF-IL-7-VNP20009 enriched within tumor. (A)** The tissue homogenate resistant plate images showed the different enrichment of GM–CSF–IL-7-VNP20009 in major organs and tumors at different time points after administration. **(B)** The number of GM–CSF–IL-7-VNP20009 clones in tumors and major organs over time (*n* = 3). Error bar, mean ± s.d. **(C)** VNP20009 16s rRNA qPCR detection reflected the amount of GM–CSF–IL-7-VNP20009 in major organs and tumors at different time points after administration (*n* = 3). Error bar, mean ± s.d. ****P < 0.0001. The statistics were analyzed by one-way ANOVA with Tukey test.

3.3. Intravenously administered GM–CSF–IL-7-VNP20009 enriched within tumor

Tumor hypoxic microenvironment suppresses the activities of immune cells, which prevents bacteria from immune surveillance [24,55]. Obligate anaerobic bacteria like *Clostridium* cannot survive in oxygenated areas but only in hypoxic tumor cores [24]. Thus, the hypoxic and necrotic tumor cores strongly support the growth of anaerobic bacteria. In order to explore whether engineered VNP20009 could target and colonize within tumors, we injected GM–CSF–IL-7-VNP20009 into B16–F10 tumor-bearing mice. Hereafter, integral organs or tissue (tumor, heart, liver, spleen, lung, kidney, brain) were homogenized in PBS to quantify the bacteria clones. The representative images of plates illustrated that the amount of bacteria in organs reached the highest point one day after GM–CSF–IL-7-VNP20009 administration and then gradually decreased from day 1 to day 21 (Fig. 3A and B). At day 21, all the bacteria in healthy organs had been cleared. But when it comes to tumors, the bacteria clones increased exponentially within 24 h, and still increased slowly in the later time (Fig. 3A and B). It was worth

mentioning that the quantification of bacterial clones showed that GM–CSF–IL-7-VNP20009 was almost 10^3 to 10^6 times enriched in tumors compared to normal organs on day 7.

In addition, we performed qPCR assay to detect VNP20009 16s rRNA expression in healthy organs and tumors at different time points. The VNP20009 16s rRNA expression level represented the relative number of bacteria. Result showed that bacteria in healthy organs increased within 3 days, and then decreased between 3 and 14 days. In contrast, bacteria in tumors remained increasing for 14 days. At 14 days, the enrichment level of GM–CSF–IL-7-VNP20009 in tumors exceeded 10^3 times that in healthy tissues (Fig. 3C). These data indicated that GM–CSF–IL-7-VNP20009 had a promising tumor-targeting capacity.

3.4. Intravenous administration of GM–CSF–IL-7-VNP20009 caused eliminable inflammation

Bacteria in blood may pose a risk of serious systemic inflammation for host. Although VNP20009 is a *Salmonella* strain attenuated to reduce inflammatory stimulation to the host, the safety of its intravenous
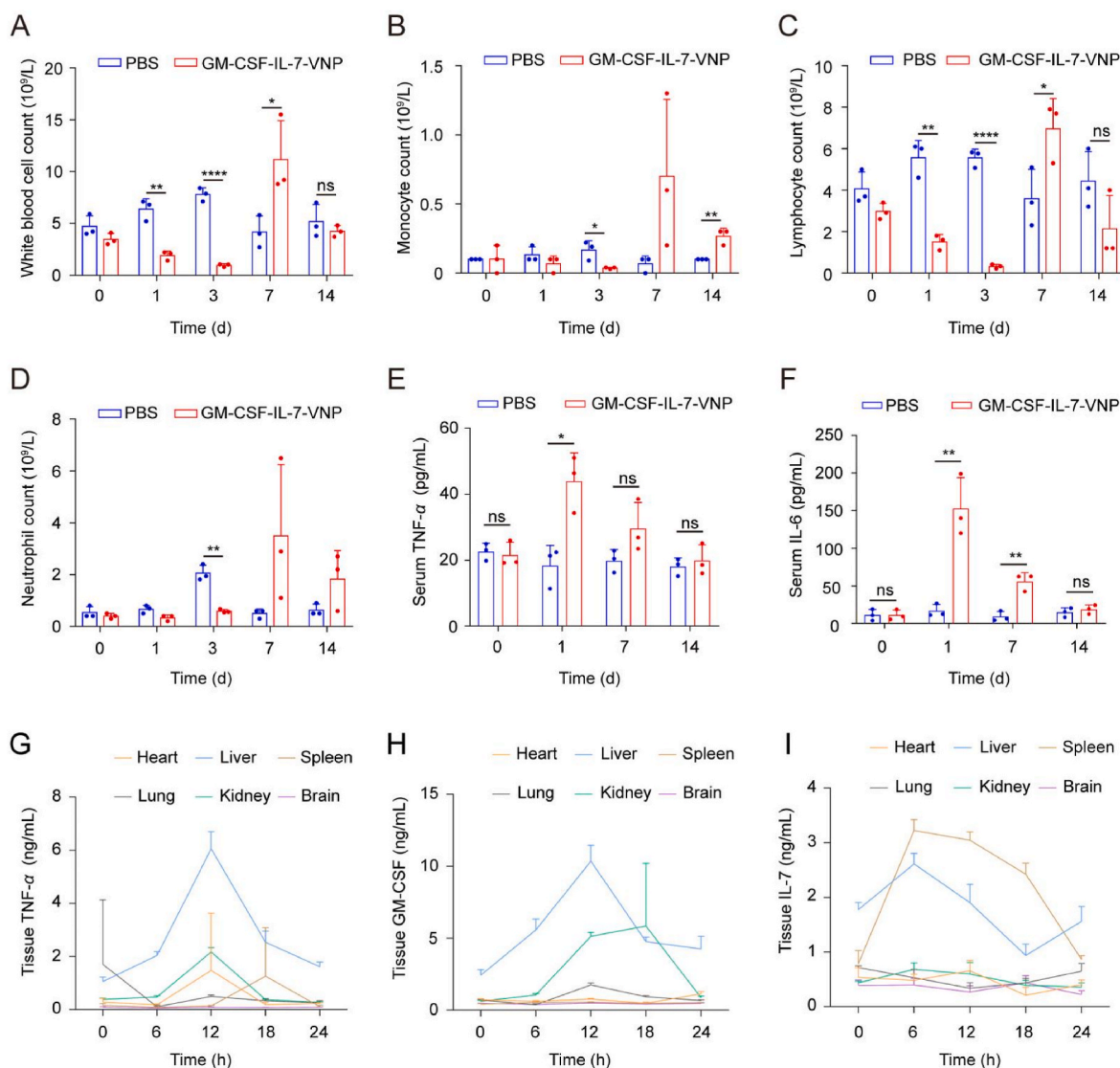
Fig. 4. Intravenous administration of GM-CSF-IL-7-VNP20009 caused eliminatable inflammation. (A) (B) (C) and (D) Blood routine test showed the concentration of white blood cell, monocyte, lymphocyte and neutrophil at different time points after GM–CSF–IL-7-VNP20009 injection ($n = 3$). Error bar, mean ± s.d. **(E) and (F)** ELISA assay showed the blood TNF-α and IL-6 concentration at different time points after GM–CSF–IL-7-VNP20009 injection ($n = 3$). Error bar, mean ± s. d. **(G) (H) and (I)** The effect of GM–CSF–IL-7-VNP20009 intravenous injection on the TNF-α, GM-CSF and IL-7 concentration in mouse tissues ($n = 3$). Error bar, mean ± s.d. *$P < 0.05$, **$P < 0.01$, ***$P < 0.001$, ****$P < 0.0001$. The statistics were analyzed by Student's *t*-test.

administration remains to be investigated. In the previous studies, we monitored the weight of treated mice and performed H&E staining of the major organs. But in order to accurately assess the systemic toxicity of GM–CSF-IL-7-VNP20009 therapy, the blood routine examination and inflammatory factors detection are necessary.

Within 14 days of 10^5 GM–CSF–IL-7-VNP20009 per mouse was injected intravenously, we detected the blood immune cell count. Results showed that the white blood cells, monocytes and lymphocytes decreased between 0 and 3 days while increased between 3 and 7 days but finally fell back on 14 days (Fig. 4A–D). Studies have shown that in the early stages of bacterial infection, immune cells decrease due to the excessive consumption. Subsequently, the immune cells increase and even continue to increase after patients' recovery from the bacterial infection [56]. Results of blood inflammatory factors detection showed that serum TNF-α and IL-6 concentrations rapidly rose between 0 and 1 days. But in 1–14 days, serum TNF-α and IL-6 concentration gradually reduced to a normal level (Fig. 4E and F). VNP20009 flagellin might stimulate TLR-5 activation and induce inflammatory cytokines

secretion, especially for TNF-α. Therefore, we also detected the changes in GM-CSF, IL-7, TNF-α and IL-6 concentrations in tissues within 24 h. Results showed that the concentrations of all these inflammatory cytokines in tissues rose within 12 h expect brain, and they reduced gradually to the level of the control within 24 h (Fig. 4G–I, Fig. S4). These data indicated that intravenous administration of GM–CSF–IL-7-VNP20009 could cause inflammation, but the inflammatory response was largely resolved within 14 days.

3.5. GM–CSF–IL-7-VNP20009 inhibited subcutaneous melanoma growth

The subcutaneous B16–F10 tumor model was employed to evaluate the anti-tumor efficacy of engineered VNP20009. Five days after B16–F10-luc cells inoculation, the tumor-bearing mice were randomly divided into 7 groups: PBS (G1), VNP20009 (G2), GM–CSF–VNP20009 (G3), IL-7-VNP20009 (G4), GM–CSF–IL-7-VNP20009 (G5), aPD-1 (G6), GM–CSF–IL-7-VNP20009 + aPD-1 (G7). For each mouse, 1×10^5 CFU engineered VNP20009 was administrated on day 0 and 2.5 mg/kg PD-1
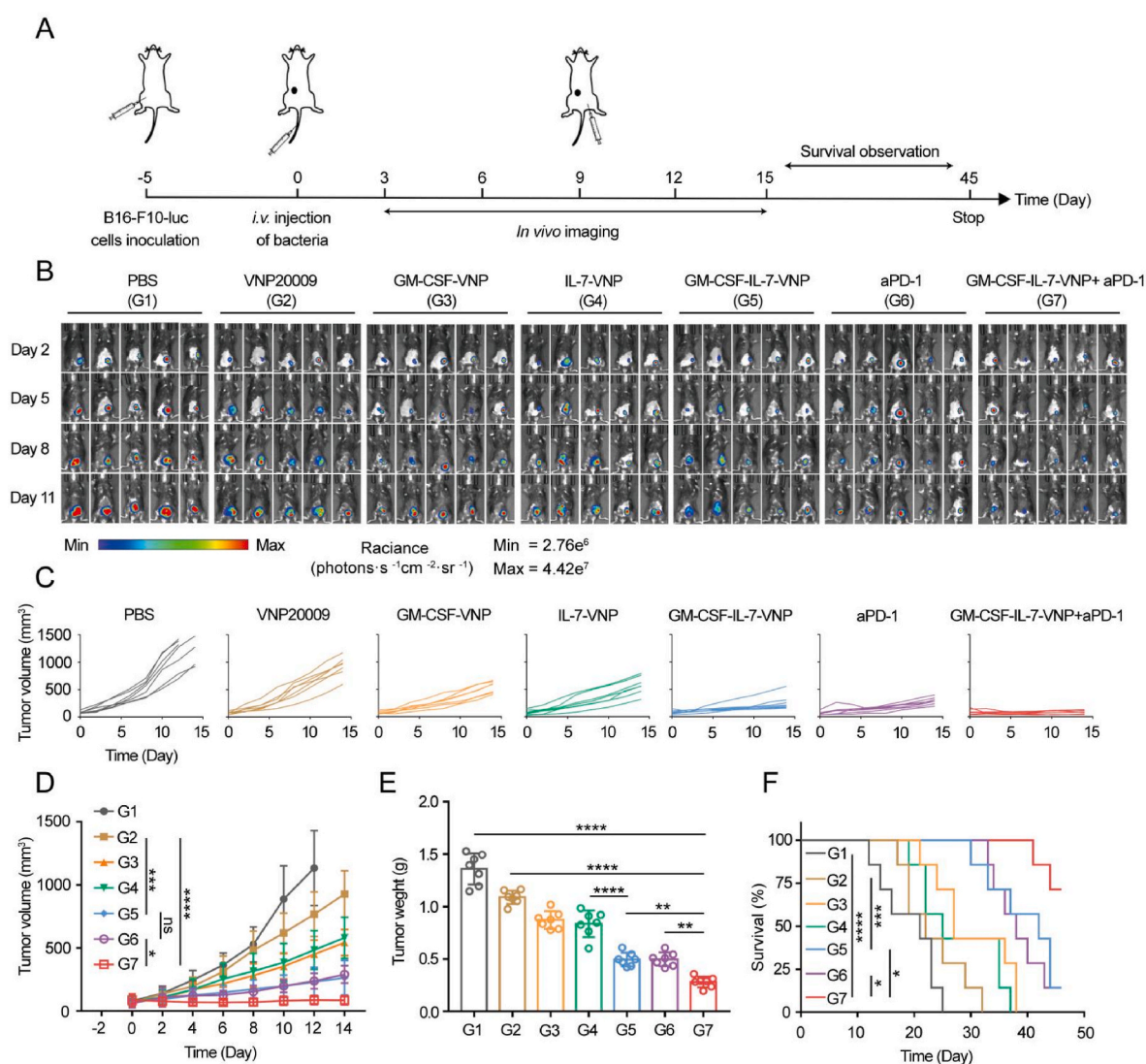
Fig. 5. Engineered VNP20009 delayed subcutaneous B16–F10-luc tumor growth *in vivo*. **(A)** Schematic illustrating the treatments given to B16–F10-luc tumor-bearing mice. **(B)** *In vivo* bioluminescence images reflecting the tumor progression of mice in different groups. **(C)** Tumor volume of a single mouse in each group. **(D)** The differences in tumor volume of all treatment groups (*n* = 7). Error bar, mean ± s.d. **(E)** Tumor weights of mice received different treatments (*n* = 7). Error bar, mean ± s.d. **(F)** Survival curves of mice received different treatments (*n* = 7). Day 0 is the day of tumor cells inoculation. (G1) PBS, (G2) VNP20009, (G3) GM–CSF–VNP20009, (G4) IL-7-VNP20009, (G5) GM–CSF-IL-7-VNP20009, (G6) aPD-1, (G7) GM–CSF–IL-7-VNP20009 plus aPD-1. ns: no significant, *$P < 0.05$, **$P < 0.01$, ***$P < 0.001$, ****$P < 0.0001$. The statistics in (D) and (E) were analyzed by one-way ANOVA with Tukey test while in (F) were analyzed by long-rank (Mantel-Cox) test.

antibody was administrated every 7 days starting on day 0 as indicated (Fig. 5A). The bioluminescence signals and tumor volumes were measured to assess the tumor progress. GM–CSF–VNP20009, IL-7-VNP20009 and GM–CSF–IL-7-VNP20009 treatment intensively restrained the tumor progress. Of note, the mice treated with GM–CSF–IL-7-VNP20009 showed stronger efficacy in delaying the

tumor progress compared to those treated with GM–CSF–VNP20009 or IL-7-VNP20009 (Fig. 5B–D). These data suggested that GM-CSF and IL-7 might have a synergistic effect in stimulating the anti-tumor response. Remarkably, the mice received GM–CSF–IL-7-VNP20009 combining with aPD-1 significantly stunted tumor growth and the tumors even remission in some mice (Fig. 5B–E). As for survival, the mice treated with
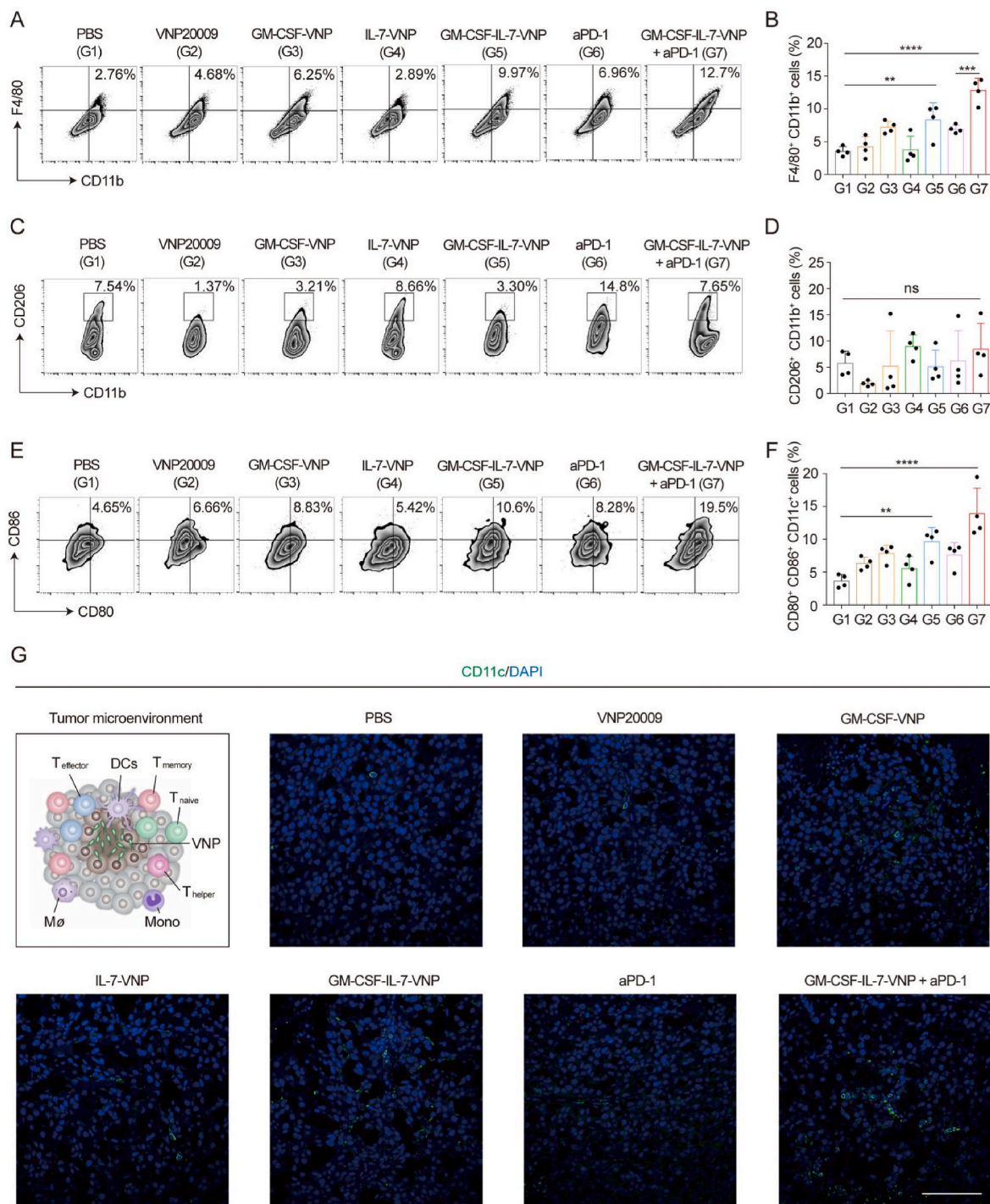
Fig. 6. GM-CSF-IL-7-VNP20009 enhanced the infiltration of macrophages and DCs into tumor. (A) and (B) Flow cytometry analysis showed the percentage of macrophages in whole tumor cell (gated out of total cells, $n = 4$). Error bar: mean $\pm$ s.d. **(C) and (D)** Flow cytometry analysis showed the percentage of M1 macrophages (gated out of CD11b$^+$ cells, $n = 4$). Error bar: mean $\pm$ s.d. **(E) and (F)** Flow cytometry analysis showed the matured DCs in whole tumor cells (gated out of total cells, $n = 4$). Error bar: mean $\pm$ s.d. **(G)** Immunofluorescence images showed the CD11c$^+$ cells within tumor tissue. (Scale bar: 100 μm). The schematic showed the engineered VNP20009 and immune cells in tumor microenvironment. T$_{naive}$: naive T cells, T$_{effector}$: effector T cells, T$_{memory}$: memory T cells, DCs: dendritic cells, Mono: monocytes, Mø: Macrophages. ns: no significant difference, *$P < 0.05$, **$P < 0.01$, ***$P < 0.001$, ****$P < 0.0001$. The statistics were analyzed by one-way ANOVA with Tukey test.

with PBS, VNP20009, GM–CSF–VNP20009 and IL-7-VNP20009 all died within 38 days after B16–F10-luc cells inoculation. Virtually, the mice treated with GM–CSF–IL-7-VNP20009 and GM–CSF–IL-7-VNP20009 combining with aPD-1 still had 57% and 71% of mice survived on day 45, achieving the benefit of extended survival (Fig. 5F). To evaluate the systemic toxicities of bacteria administration, we measured the body weights of mice in different groups. Cytokines therapy is not tumor targeted, cytokines are usually not possible to build up effective concentration at the tumor site after administration. GM–CSF–IL-7-VNP20009 had the ability of targeting tumor, and secreting GM-CSF and IL-7, which might facilitate the higher cytokines concentration accumulation, resulting in better anti-tumor efficacy. Here, we compared the antitumor effect of the cytokines therapy and GM–CSF–IL-7-VNP20009 therapy on subcutaneous melanoma model. GM-CSF and IL-7 were both injected intravenously at 5 μg/kg concentration every day. We recorded the tumor volumes during treatment , and the results showed that the GM–CSF–IL-7-VNP20009 therapy had a better tumor inhibition ability than the cytokines therapy (Fig. S5). The average body weights of mice in each group had no significant loss, indicating no apparent systemic toxicities during the treatment period (Fig. S6). The hematoxylin-eosin (H&E) staining images showed no obvious damage in the major organs of the treated mice (Fig. S7).

3.6. GM–CSF–IL-7-VNP20009 enhanced macrophages and DCs infiltration

The tumors of mice that received different treatments were harvested on day 14, and then were prepared as single-cell suspensions for flow cytometry analysis to explore the tumor-infiltrating immune cells. Tumor-infiltrating macrophages have the ability of phagocytosis and antigen presentation, which is closely related to tumor progression. M1 macrophages secrete pro-inflammatory cytokines such as IL-12 and IL-23, produce tumor cell killing molecules such as ROS and NO. But in contrast, M2 macrophages secrete immunosuppressive factors such as IL-10, TGF-β, which is associated with tumor cell proliferation and metastasis. First, the CD11b and F4/80 double positive cells were distinguished to macrophages. Further, the CD80 and CD86 double positive cells were classified as M1 macrophages, while CD206 positive cells were classified as M2 macrophages. As shown in Fig. 6A and B, GM–CSF–VNP20009, aPD-1, GM–CSF–IL-7-VNP20009, and GM–CSF–IL-7-VNP20009 plus aPD-1 treatment increased the percentage of macrophages out of whole tumor cell. Then, we further subtyped these macrophages. As shown in Figs. S8A and B, the proportion of M1 macrophages was increased in the GM–CSF–IL-7-VNP20009 plus aPD-1 group, but no significant difference was observed. At the same time, there was no significant difference in the proportion of M2 macrophages between groups (Fig. 6C and D). These results suggest that GM-CSF secreted by engineered VNP20009 mainly enhanced the infiltration of macrophages into tumors, but had no significant effect on the M1 or M2 polarization of macrophages.

DCs are the most important antigen-presenting cells for activating anti-tumor immunity. Mature DCs highly express CD80 and CD86, the T cell costimulatory molecules that activate the initial T cell response. We analyzed the number of tumor-infiltrating DCs by flow cytometry and immunofluorescence staining assays. Compared with PBS treatment, VNP20009, GM–CSF–VNP20009, GM–CSF–IL-7-VNP20009 and GM–CSF–IL-7-VNP20009 plus aPD-1 treatments increased the percentage of tumor-infiltrating mature DCs (Fig. 6E and F). In addition, immunofluorescence images of tumor tissue also showed more CD11c$^+$ cell infiltration in the GM–CSF–VNP20009, GM–CSF–IL-7-VNP20009 and GM–CSF–IL-7-VNP20009 plus aPD-1 groups (Fig. 6G). These results suggested that single VNP20009 treatment could enhance mature DCs infiltration to a certain extent, and the effect was further enhanced because of the GM-CSF secretion.

3.7. GM–CSF–IL-7-VNP20009 enhanced T cell anti-tumor response

Increasing T cell infiltration and activation is pivotal to solid tumor immunotherapy. Various helper T cells derived from the initial CD4$^+$ T cells produce pro-immune cytokines and enhance the activity of CD8$^+$ T cells. Hereafter CD8$^+$ T cells recognize and eliminate tumor cells. Firstly, we analyzed the percentage of CD3$^+$CD4$^+$ T cells and CD3$^+$CD8$^+$ T cells out of the whole tumor. Compared with the PBS treatment, GM–CSF–IL-7-VNP20009 treatment significantly increased the percentage of tumor-infiltrating CD4$^+$ T cells and CD8$^+$ T cells (Fig. 7A–D). The aPD-1 treatment increased CD8$^+$ T cell infiltration but had no significant effect on CD4$^+$ T cells. Notably, compared with the single aPD-1 treatment, when we combined the GM–CSF–IL-7-VNP20009 with aPD-1 administration, the CD8$^+$ T cell infiltration was further enhanced. Interestingly, we observed that wild-type VNP20009 administration also sightly increased the percentage of tumor-infiltrating CD4$^+$ T cells. It has been demonstrated that CD4$^+$ T cells are the main cells that protect mice from *Salmonella* infection [57]. This CD4$^+$ T cell population is specific to *Salmonella* flagella protein (FliC) and produces high levels of IFN-γ, which might also exert anti-tumor activity [57,58].

Tumor-specific CD8$^+$ T cells generate perforin, granzyme B (GZMB), IFN-γ and TNF-α to directly eliminate tumor cells [59]. Therefore, we also detected these molecules in tumor-infiltrating CD8$^+$ T cells. After being treated with GM–CSF–IL-7-VNP20009, the GZMB$^+$, IFN-γ^+ and TNF-α^+ CD8$^+$ T cells in CD8$^+$ T cell population elevated significantly compared to those mice only received VNP20009 treatment. What's more, for the mice that received GM–CSF–IL-7-VNP20009 combined with aPD-1, the IFN-γ^+ CD8$^+$ T and TNF-α^+ CD8$^+$ T cell populations were further increased (Fig. 7E and F, Figs. S9A–F).

In addition, tumor-infiltrating CD4$^+$ T and CD8$^+$ T cells were visualized by immunofluorescence staining assay. We stained both CD4 and CD8 proteins within tumor tissues. The confocal images showed that the CD8$^+$ T cell infiltration were facilitated in the mice treated with GM–CSF–IL-7-VNP20009, aPD-1 and GM–CSF–IL-7-VNP20009 plus aPD-1. While for CD4$^+$ T cells, the tumor tissues of mice treated with IL-7-VNP20009, GM–CSF–IL-7-VNP20009 and GM–CSF–IL-7-VNP20009 plus aPD-1 were observed an enhanced infiltration compared to the mice treated with PBS (Fig. 7G and H, Fig. S10).

These data demonstrated that the GM–CSF–IL-7-VNP20009 treatment could mediate T cell expansion and activation in solid tumor. The additional aPD-1 further enhanced T cell anti-tumor response, preferably restrain the tumor growth.

3.8. GM–CSF–IL-7-VNP20009 protected mice from lung metastatic melanoma

After intravenous injection, the engineered VNP20009 specifically targeted tumors and proliferated within tumors throughout the body, which made it possible to employ GM–CSF–IL-7-VNP20009 to treat malignant metastatic tumors. In order to evaluate the capacity of GM–CSF–IL-7-VNP20009 in treating lung metastatic melanoma, we injected 1×10^5 B16–F10-luc cells intravenously into each mouse. Five days later, we treated each mouse with 1×10^5 CFU engineered VNP20009, and the aPD-1 was administrated every 7 days (Fig. 8A). The bioluminescence images reflected the lung metastatic tumor growth. As the images showed, the mice treated with GM–CSF–IL-7-VNP20009 combining aPD-1 had the strongest capacity in delaying tumor progress. Mice treated with GM–CSF–VNP20009 or IL-7-VNP20009 did not exhibit significantly reduced tumor burden compared to those mice treated with VNP20009 (Fig. 8B). When it reached 15 day, the whole lungs of mice were obtained for melanoma metastases quantification and H&E staining analysis. We found that the numbers of lung metastasis nodes of mice with different treatments were basically consistent with the trends shown in bioluminescence images (Fig. 8C). What's more, the melanoma metastases were shown as dark purple dense tissues in H&E images. The numbers and sizes of melanoma metastases in the
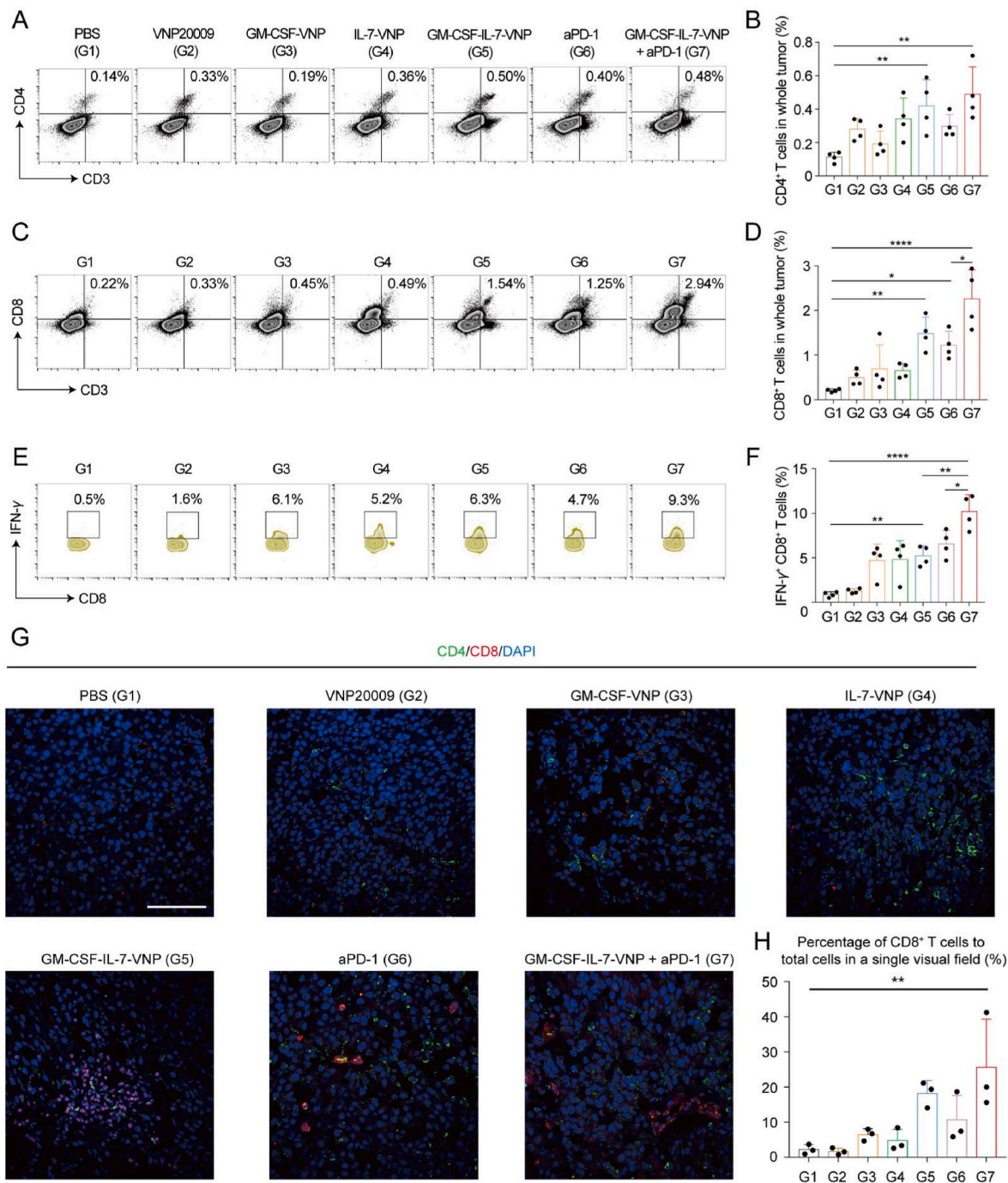
Fig. 7. GM-CSF-IL-7-VNP20009 promoted the infiltration and anti-tumor activity of T cells. (A) and (B) Flow cytometry analysis showed the percentage of CD4$^+$ T cells in whole tumor cell (gated out of total cells, $n = 4$). Error bar: mean $\pm$ s.d. (C) and (D) Flow cytometry analysis showed the percentage of CD8$^+$ T cells in whole tumor cell (gated out of total cells, $n = 4$). Error bar: mean $\pm$ s.d. (E) and (F) Flow cytometry analysis showed the percentage of IFN-γ^+ CD8$^+$ T cells (gated out of CD3$^+$ cells, $n = 4$). Error bar: mean $\pm$ s.d. (G) Representative immunofluorescence images showed the CD4$^+$ T cells and CD8$^+$ T cells within tumor tissue. (Scale bar: 100 µm). (H) Count of CD8$^+$ T cells in a single visual field ($n = 3$). Error bar, mean $\pm$ s.d. *$P < 0.05$, **$P < 0.01$, ***$P < 0.001$, ****$P < 0.0001$. The statistics were analyzed by one-way ANOVA with Tukey test.

lungs of mice treated with GM–CSF–IL-7-VNP20009, aPD-1 and GM–CSF–IL-7-VNP20009 plus aPD-1 were much lower than those mice treated with PBS and VNP20009 (Fig. 8D). For survival, the mice that received PBS, VNP20009, GM-CSF-VNP20009 and IL-7-VNP20009 treatments were all died within 31 day, respectively. In contrast, the mice treated with GM–CSF–IL-7-VNP20009, aPD-1 and GM–CSF–IL-7-VNP20009 plus aPD-1 still had 43%, 29% and 86% of the mice keeping alive, respectively (Fig. 8E). Combining administration of aPD-1 with GM–CSF–IL-7-VNP20009 intensively prolonged the survival in mice.

The body weights of mice that received different treatments were basically stable during the treatment period, indicating the safety of living bacteria administration (Fig. 8F). These data demonstrated that GM–CSF–IL-7-VNP20009 in combination with aPD-1 showed a considerable therapeutic effect in suppressing the melanoma metastasis.

The suppression of lung metastatic tumor may be dependent on the circulating tumor-specific CD8$^+$ T cells. Therefore, we used Trp-2 (a melanoma cell antigen) specific MHC tetramer to interact with circulating Trp-2-specific CD8$^+$ T cells. Whole blood of the treated mice was
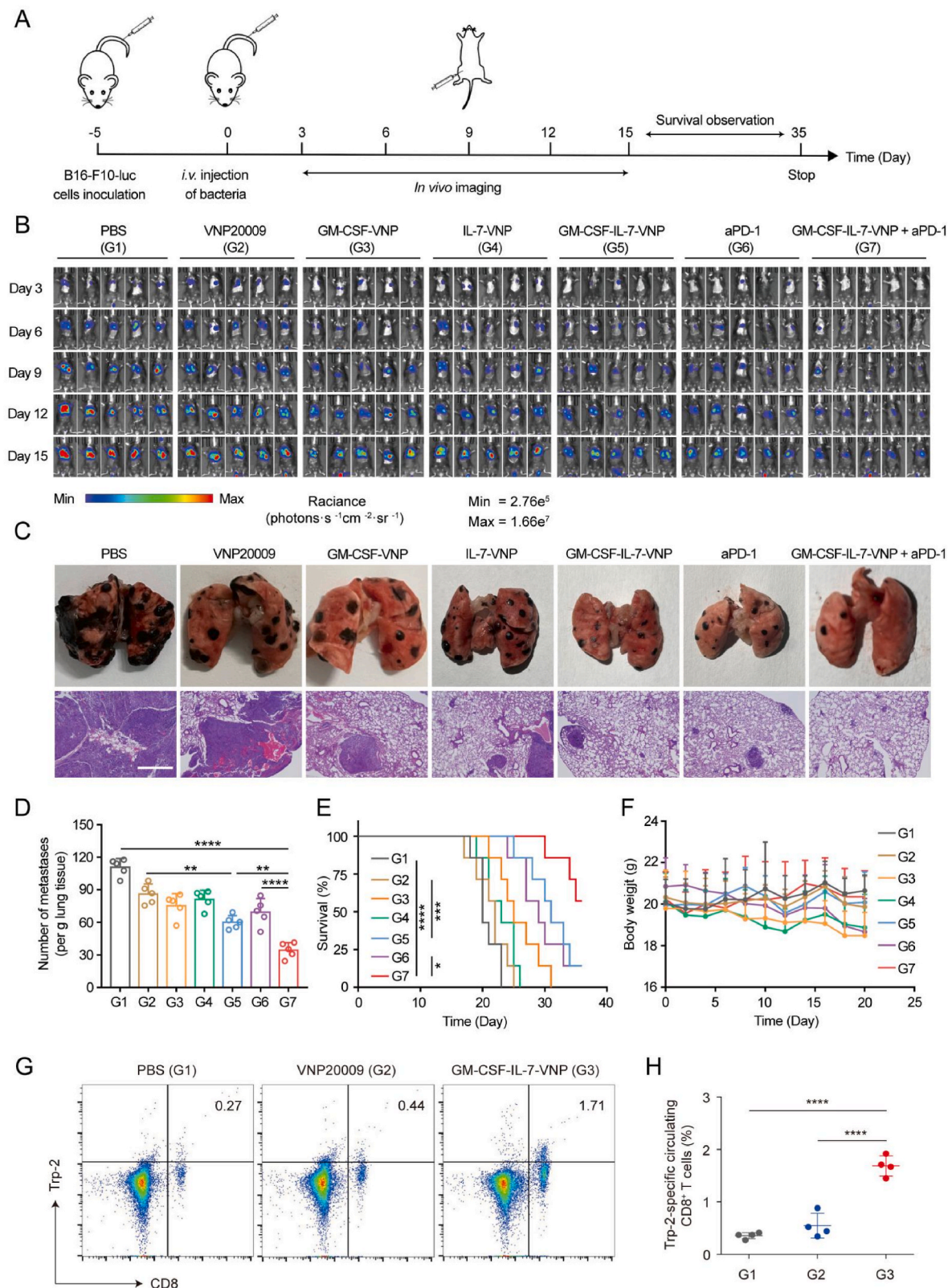
Fig. 8. Engineered VNP20009 suppressed the lung metastatic melanoma progress. (A) Schematic showing the treatments the B16–F10-luc tumor-bearing mice received. **(B)** *In vivo* bioluminescence images showing the lung metastatic melanoma progression of mice received different treatments. **(C)** Representative lung images and H&E staining images reflecting the severity of lung metastases in different groups. (Scale bar: 200 μm). **(D)** The quantification of the lung metastases in different groups ($n = 5$). Error bar: mean ± s.d. **(E)** Survival curves of mice received different treatments ($n = 7$). Day 0 was the day of B16–F10-luc cells inoculation. **(F)** Body weights of mice received different treatments ($n = 5$). Error bar, mean ± s.d. **(G) and (H)** Flow cytometry showed the percentage of Trp-2-specific CD8$^+$ T cells out of the whole blood cell ($n = 4$). Error bar, mean ± s.d. *$P < 0.05$, **$P < 0.01$, ***$P < 0.001$, ****$P < 0.0001$. The statistics in (D) (F) and (H) were analyzed by one-way ANOVA with Tukey test while in (E) were analyzed by long-rank (Mantel-Cox) test.

harvested for flow cytometry analysis. Results had shown that GM–CSF–IL-7-VNP20009 treatment significantly increased the Trp-2-specific CD8$^+$ T cells in blood, which might contribute to the distal tumor elimination (Fig. 8G and H).

4. Discussion

In summary, we constructed an attenuated *Salmonella* VNP20009 strain that was capable of targeting tumors and secreting GM-CSF and IL-7. Bacteria-secreted GM-CSF and IL-7 enhanced macrophages, DCs infiltration and T cell activation, showing a notable anti-tumor efficacy. Furthermore, when given additional PD-1 antibody, the tumor-bearing mice achieved more therapeutic benefits, illustrating the combined potential of GM–CSF–IL-7-VNP20009 and immune checkpoint blocking antibodies in the treatment of tumors. Although IL-7 has been used to treat tumors in previous studies, there were also studies indicated that IL-7 might promote tumor progression and metastasis [60,61]. In prostate cancer, low IL-7 and IL-7 receptor expression is predictive of poor prognosis and the IL-7 vaccine is proved to enhance CD4$^+$ T cell, CD8$^+$ T cell and CD19$^+$ B cell infiltration [62]. However, in T cell acute lymphoblastic leukemia (T-ALL), high IL-7 receptor expression was detected on the malignant T cells [63]. In various leukemia, IL-7 endows malignant cells with resistance to anti-cancer drugs such as adriamycin, rapamycin and imatinib by inhibiting cell apoptosis [64–66]. Therefore, when using engineered bacteria to deliver IL-7, it is necessary to take into account the appropriate cancer types and reduce the IL-7 leakage. With the invention of more complex genetic circuits such as self-cracking system, it is expected to achieve local concentration control of engineered bacterial delivery drugs in the future, further reducing drug side effects.

Current cancer research has long sought a novel method that could selectively target and kill malignant cells in contrast to the traditional therapies. Due to the inherent tumor targeting ability and highly editable genomes, anaerobic bacteria have been widely explored for cancer immunotherapy. The bacterial colonization within tumor induces persistent and complicated immune response, which is essential for tumor regression. Macrophages, neutrophils and NK cells, which are part of innate immunity, are the first to respond to bacterial infections. Cytokines released during this process contribute to the arousal of adaptive immunity. Bacillus Calmette–Guérin (BCG) is the first bacterial cancer therapy approved for clinical use [23]. Recently, Anthony C. Antonelli et al. have found that BCG-induced tumor remission is dependent on IFN-γ-generating CD4$^+$ T cells [67]. In addition, Alejandrina Vendrell et al. have found that *Salmonella* can enhance the Th1-type cellular immune response, leading increased frequencies of IFN-γ-secreting CD4$^+$ and CD8$^+$ T cells [68]. However, such inflammation may also bring unacceptable inflammatory adverse effects to the host. In this study, we found that although the toxicity of VNP20009 was attenuated, it could still cause short-term blood and tissue inflammation. How to minimize the toxicity while taking into account the anti-cancer ability of bacteria is an urgent issue of bacterial immunotherapy. Tetsuhiro Harimoto et al. have engineered *E. coli* Nissle 1917 (EcN) to synthesis bacterial surface capsular polysaccharide (CAP) [38]. These bacteria can temporarily evade immune attack, whereas subsequent loss of CAP can lead to rapidly clearance *in vivo*. This strategy increases the maximum tolerance dose of the host to bacteria by ten times. With the continuous elucidation of tumor biomarkers, it is also of great significance to search for bacterial mutants that only survive in tumors [69].

The powerful tumor colonization and immune arousal ability of bacteria attract researches' interest to combine bacteria with other cancer immunotherapies. Gang Xin et al. have decorated tumor-specific CD8$^+$ T cells with a second T-cell receptor (TCR) to recognize a bacterial antigen. Intratumoral injection of bacteria enhances the migration of adoptive T cells to tumors [70]. What's more, the potential of the combination of bacterial immunotherapy and immune checkpoint antibodies is being evaluated [28]. Tumor-targeting bacteria are expected to bring new breakthroughs for tumor targeted therapy in the future.

5. Conclusions

In summary, we constructed an attenuated *Salmonella* VNP20009 strain capable of targeting tumor and secreting therapeutic cytokines *in situ*. After the L-arabinose induction, engineered VNP20009 secreted mouse GM-CSF and IL-7 within tumors. The GM-CSF recruits DCs for T cell priming, while the IL-7 promoted the survival and proliferation of tumor-infiltrating T cells and memory T cells. The synergy of GM-CSF and IL-7 enhanced the infiltration and vitality of immune cells in TME. More importantly, the combined administration of GM–CSF–IL-7-VNP20009 and aPD-1 received better therapeutic benefits than either alone. Thus, live bacteria such as VNP20009 capable of targeting tumor to synthetize therapeutic molecules *in situ* could be a promising strategy for solid tumor immunotherapy.

CRediT authorship contribution statement

Zhongda Lin: performed the experiments, interpreted the data, wrote the paper. The manuscript was written through contributions of all authors. All authors have given approval to the final version of the manuscript. **Fanqiang Meng:** performed the experiments, interpreted the data. The manuscript was written through contributions of all authors. All authors have given approval to the final version of the manuscript. **Yumeng Ma:** performed the experiments. The manuscript was written through contributions of all authors, All authors have given approval to the final version of the manuscript. **Chi Zhang:** performed the experiments, The manuscript was written through contributions of all authors, All authors have given approval to the final version of the manuscript. **Zhirang Zhang:** performed the experiments, The manuscript was written through contributions of all authors, All authors have given approval to the final version of the manuscript. **Zhaoxin Yang:** performed the experiments, The manuscript was written through contributions of all authors, All authors have given approval to the final version of the manuscript. **Yuan Li:** performed the experiments, The manuscript was written through contributions of all authors, All authors have given approval to the final version of the manuscript. **Linlin Hou:** performed the experiments, The manuscript was written through contributions of all authors, All authors have given approval to the final version of the manuscript. **Yuzhong Xu:** The manuscript was written through contributions of all authors, All authors have given approval to the final version of the manuscript. **Xin Liang:** designed the study, The manuscript was written through contributions of all authors, All authors have given approval to the final version of the manuscript. **Xudong Zhang:** designed the study, wrote the paper. The manuscript was written through contributions of all authors. All authors have given approval to the final version of the manuscript.

Declaration of competing interest

The authors declare that no competing interests exist.

Appendix A. Supplementary data

Supplementary data to this article can be found online at https://doi.org/10.1016/j.bioactmat.2023.09.007.

References

[1] A.C. Huang, R. Zappasodi, A decade of checkpoint blockade immunotherapy in melanoma: understanding the molecular basis for immune sensitivity and resistance, Nat. Immunol. 23 (2022) 660–670.
[2] C. Robert C, et al., Pembrolizumab versus ipilimumab in advanced melanoma, N. Engl. J. Med. 372 (2015) 2521–2532.
[3] A.J. Korman, S.C. Garrett-Thomson, N. Lonberg, The foundations of immune checkpoint blockade and the ipilimumab approval decennial, Nat. Rev. Drug Discov. 21 (2022) 509–528.
[4] G. Morad, B.A. Helmink, P. Sharma, J.A. Wargo, Hallmarks of response, resistance, and toxicity to immune checkpoint blockade, Cell 185 (2022) 576.
[5] A. Kalbasi, A. Ribas, Tumour-intrinsic resistance to immune checkpoint blockade, Nat. Rev. Immunol. 20 (2020) 25–39.
[6] J. Ni, Z. Zhang, M. Ge, J. Chen, W. Zhuo, Immune-based combination therapy to convert immunologically cold tumors into hot tumors: an update and new insights, Acta Pharmacol. Sin. 44 (2022) 288–307.
[7] T.N. Schumacher, R.D. Schreiber, Neoantigens in cancer immunotherapy, Science 348 (2015) 69–74.
[8] A. Facciabene, et al., Tumour hypoxia promotes tolerance and angiogenesis via CCL28 and T(reg) cells, Nature 475 (2011) 226–230.
[9] N. Nagarsheth, M.S. Wicha, W. Zou, Chemokines in the cancer microenvironment and their relevance in cancer immunotherapy, Nat. Rev. Immunol. 17 (2017) 559–572.
[10] H.L. Kaufman, F.J. Kohlhapp, A. Zloza, Oncolytic viruses: a new class of immunotherapy drugs, Nat. Rev. Drug Discov. 14 (2015) 642–662.
[11] L. Fu, et al., Recent advances in oncolytic virus-based cancer therapy, Virus Res. 270 (2019) 197675.
[12] D.B. Johnson, I. Puzanov, M.C. Kelley, Talimogene laherparepvec (T-VEC) for the treatment of advanced melanoma. Immunotherapy, Immunotherapy-Uk 7 (2015) 611–619.
[13] K. Harrington, D.J. Freeman, B. Kelly, J. Harper, J.C. Soria, Optimizing oncolytic virotherapy in cancer treatment, Nat. Rev. Drug Discov. 18 (2019) 689–706.
[14] S.J. Russell, K.W. Peng, Oncolytic virotherapy: a contest between apples and oranges, Mol. Ther. 25 (2017) 1107–1116.
[15] J. Chesney, et al., Randomized, open-label phase II study evaluating the efficacy and safety of talimogene laherparepvec in combination with ipilimumab versus ipilimumab alone in patients with advanced, unresectable melanoma, J. Clin. Oncol. 36 (2018) 1658–1667.
[16] K.J. Harrington, et al., Talimogene laherparepvec and pembrolizumab in recurrent or metastatic squamous cell carcinoma of the head and neck (MASTERKEY-232): a multicenter, phase 1b study, Clin. Cancer Res. 26 (2020) 5153–5161.
[17] C.J. Breitbach, et al., Intravenous delivery of a multi-mechanistic cancer-targeted oncolytic poxvirus in humans, Nature 477 (2011) 99–102.
[18] T.C. Liu, D. Kirn, Systemic efficacy with oncolytic virus therapeutics: clinical proof-of-concept and future directions, Cancer Res. 67 (2007) 429–432.
[19] P.K. Bommareddy, M. Shettigar, H.L. Kaufman, Integrating oncolytic viruses in combination cancer immunotherapy, Nat. Rev. Immunol. 18 (2018) 498–513.
[20] A. Fu, et al., Tumor-resident intracellular microbiota promotes metastatic colonization in breast cancer, Cell 185 (2022) 1356–1372.
[21] A. Wong-Rolle, H.K. Wei, C. Zhao, C. Jin, Unexpected guests in the tumor microenvironment: microbiome in cancer, Protein Cell 12 (2021) 426–435.
[22] E.F. McCarthy, The toxins of William B. Coley and the treatment of bone and soft-tissue sarcomas, Iowa Orthop. J. 26 (2006) 154–158.
[23] C. Lange, et al., 100 years of Mycobacterium bovis bacille Calmette-Guérin, Lancet Infect. Dis. 22 (2022) e2–e12.
[24] M.T. Duong, Y. Qin, S. You, J. Min, Bacteria-cancer interactions: bacteria-based cancer therapy, Exp. Mol. Med. 51 (2019) 1–15.
[25] K. Kim, et al., L-Asparaginase delivered by Salmonella typhimurium suppresses solid tumors, Molecular Therapy - Oncolytics 2 (2015), 15007.
[26] C.R. Gurbatri, et al., Engineered probiotics for local tumor delivery of checkpoint blockade nanobodies, Sci. Transl. Med. 12 (2020) 530.
[27] S. Chowdhury, et al., Programmable bacteria induce durable tumor regression and systemic antitumor immunity, Nat. Med. 25 (2019) 1057–1063.
[28] S. Zhou, C. Gravekamp, D. Bermudes, K. Liu, Tumour-targeting bacteria engineered to fight cancer, Nat. Rev. Cancer 18 (2018) 727–743.
[29] M. Loeffler, G. Le'Negrate, M. Krajewska, J.C. Reed, Attenuated salmonella engineered to produce human cytokine light inhibit tumor growth, Proceedings of the National Academy of Sciences - PNAS 104 (2007) 12879–12883.
[30] C. Xing, et al., Microbiota regulate innate immune signaling and protective immunity against cancer, Cell Host Microbe 29 (2021) 959–974.
[31] M.H. Abedi, et al., Ultrasound-controllable engineered bacteria for cancer immunotherapy, Nat. Commun. 13 (2022).
[32] K. Westphal, S. Leschner, J. Jablonska, H. Loessner, S. Weiss, Containment of tumor-colonizing bacteria by host neutrophils, Cancer Res. 68 (2008) 2952–2960.
[33] R.M. Salazar-Gonzalez, S.J. McSorley, Salmonella flagellin, a microbial target of the innate and adaptive immune system, Immunol. Lett. 101 (2005) 117–122.
[34] L. Sfondrini, et al., Antitumor activity of the TLR-5 ligand flagellin in mouse models of cancer, J. Immunol. 176 (2006) 6624–6630.
[35] A. Cubillos-Ruiz, et al., Engineering living therapeutics with synthetic biology, Nat. Rev. Drug Discov. 20 (2021) 941–960.
[36] M.P. McNerney, K.E. Doiron, T.L. Ng, T.Z. Chang, P.A. Silver, Theranostic cells: emerging clinical applications of synthetic biology, Nat. Rev. Genet. 22 (2021) 730–746.
[37] X.N. Wang, M.T. Niu, J.X. Fan, Q.W. Chen, X.Z. Zhang, Photoelectric bacteria enhance the in situ production of tetrodotoxin for antitumor therapy, Nano Lett. 21 (2021) 4270–4279.
[38] Q.W. Chen, et al., Self-mineralized photothermal bacteria hybridizing with mitochondria-targeted metal–organic frameworks for augmenting photothermal tumor therapy, Adv. Funct. Mater. 30 (2020), 1909806.
[39] T. Harimoto, et al., A programmable encapsulation system improves delivery of therapeutic bacteria in mice, Nat. Biotechnol. 40 (2022) 1259–1269.
[40] V. Raman, et al., Intracellular delivery of protein drugs with an autonomously lysing bacterial system reduces tumor growth and metastases, Nat. Commun. 12 (2021) 6116.
[41] M.O. Din, et al., Synchronized cycles of bacterial lysis for in vivo delivery, Nature 536 (2016) 81–85.
[42] Y. Chen, M. Du, Z. Yuan, Z. Chen, F. Yan, Spatiotemporal control of engineered bacteria to express interferon-γ by focused ultrasound for tumor immunotherapy, Nat. Commun. 13 (2022).
[43] N.S. Forbes, Engineering the perfect (bacterial) cancer therapy, Nat. Rev. Cancer 10 (2010) 785–794.
[44] K. Liang, et al., Genetically engineered Salmonella Typhimurium: recent advances in cancer therapy, Cancer Lett. 448 (2019) 168–181.
[45] B. Becher, S. Tugues, M. Greter, GM-CSF: from growth factor to central mediator of tissue inflammation, Immunity 45 (2016) 963–973.
[46] J.A. Hamilton, GM-CSF in inflammation, J. Exp. Med. 217 (2020).
[47] G. Dranoff, et al., Vaccination with irradiated tumor cells engineered to secrete murine granulocyte-macrophage colony-stimulating factor stimulates potent, specific, and long-lasting anti-tumor immunity, Proc. Natl. Acad. Sci. U. S. A. 90 (1993) 3539–3543.
[48] C. Luu, N.I. Khushalani, J.S. Zager, Intralesional and systemic immunotherapy for metastatic melanoma, Expet Opin. Biol. Ther. 16 (2016) 1491–1499.
[49] B. Arneth, Tumor microenvironment, Medicina (Kaunas) 56 (2019) 15.
[50] J. Lin, et al., The role of IL-7 in immunity and cancer, Anticancer Res. 37 (2017) 963–968.
[51] D.H. Lynch, A.E. Namen, R.E. Miller, In vivo evaluation of the effects of interleukins 2, 4 and 7 on enhancing the immunotherapeutic efficacy of anti-tumor cytotoxic T lymphocytes. Eur J Immunol, Eur. J. Immunol. 21 (1991) 2977–2985.
[52] B. Habenstein, et al., Structures of type III secretion system needle filaments, Curr. Top. Microbiol. Immunol. 427 (2020) 109–131.
[53] F. Sallusto, A. Lanzavecchia, Efficient presentation of soluble antigen by cultured human dendritic cells is maintained by granulocyte/macrophage colony-stimulating factor plus interleukin 4 and downregulated by tumor necrosis factor alpha, J. Exp. Med. 179 (1994) 1109–1118.
[54] J. Helft, et al., GM-CSF mouse bone marrow cultures comprise a heterogeneous population of CD11c (+) MHCII (+) macrophages and dendritic cells, Immunity 42 (2015) 1197–1211.
[55] T. Hompland, C.S. Fjeldbo, H. Lyng, Tumor hypoxia as a barrier in cancer therapy: why levels matter, Cancers 13 (2021).
[56] T. Honda, T. Uehara, G. Matsumoto, S. Arai, M. Sugano, Neutrophil left shift and white blood cell count as markers of bacterial infection, Clin. Chim. Acta 457 (2016) 46–53.
[57] S.J. McSorley, B.T. Cookson, M.K. Jenkins, Characterization of CD4+ T cell responses during natural infection with Salmonella typhimurium, J. Immunol. 164 (2000) 986–993.
[58] M.B. Sztein, et al., Cytokine production patterns and lymphoproliferative responses in volunteers orally immunized with attenuated vaccine strains of Salmonella typhi, J. Infect. Dis. 170 (1994) 1508–1517.
[59] P.M. St, P.S. Ohashi, The roles of CD8+ T cell subsets in antitumor immunity, Trends Cell Biol. 30 (2020) 695–704.
[60] M.A. Seol, et al., Interleukin-7 contributes to the invasiveness of prostate cancer cells by promoting epithelial-mesenchymal transition, Sci. Rep. 9 (2019) 6917.
[61] S.L. Park, E.J. Lee, W.J. Kim, S.K. Moon, p27KIP1 is involved in ERK1/2-mediated MMP-9 expression via the activation of NF-κB binding in the IL-7-induced migration and invasion of 5637 cells, Int. J. Oncol. 44 (2014) 1349–1356.
[62] C. Schroten-Loef, et al., A prostate cancer vaccine comprising whole cells secreting IL-7, effective against subcutaneous challenge, requires local GM-CSF for intra-prostatic efficacy, Cancer Immunol. Immunother. 58 (2009) 373–381.
[63] I. Dibirdik, et al., Engagement of interleukin-7 receptor stimulates tyrosine phosphorylation, phosphoinositide turnover, and clonal proliferation of human T-lineage acute lymphoblastic leukemia cells, Blood 78 (1991) 564–570.
[64] L. Cattaruzza, et al., Functional coexpression of Interleukin (IL-7) and its receptor (IL-7R) on Hodgkin and Reed-Sternberg cells: involvement of IL-7 in tumor cell

growth and microenvironmental interactions of Hodgkin's lymphoma, Int. J. Cancer 125 (2009) 1092–1101.

[65] A. Kariminia, et al., Y-box-binding protein 1 contributes to IL-7-mediated survival signaling in B-cell precursor acute lymphoblastic leukemia, Oncol. Lett. 13 (2017) 497–505.

[66] V.I. Brown, et al., Rapamycin is active against B-precursor leukemia in vitro and in vivo, an effect that is modulated by IL-7-mediated signaling, Proc. Natl. Acad. Sci. U. S. A. 100 (2003) 15113–15118.

[67] A.C. Antonelli, A. Binyamin, T.M. Hohl, M.S. Glickman, G. Redelman-Sidi, Bacterial immunotherapy for cancer induces CD4-dependent tumor-specific

immunity through tumor-intrinsic interferon-γ signaling, Proc. Natl. Acad. Sci. U. S. A. 117 (2020) 18627–18637.

[68] A. Vendrell, et al., A novel salmonella typhi-based immunotherapy promotes tumor killing via an antitumor th1-type cellular immune response and neutrophil activation in a mouse model of breast cancer, Vaccine 29 (2011) 728–736.

[69] M. Zhao, et al., Tumor-targeting bacterial therapy with amino acid auxotrophs of GFP-expressing Salmonella typhimurium, Proc. Natl. Acad. Sci. U. S. A. 102 (2005) 755–760.

[70] G. Xin, et al., Pathogen boosted adoptive cell transfer immunotherapy to treat solid tumors, Proc. Natl. Acad. Sci. USA 114 (2017) 740–745.